COMPDYN 2011
III ECCOMAS Thematic Conference on
Computational Methods in Structural Dynamics and Earthquake Engineering
M. Papadrakakis, M. Fragiadakis, V. Plevris (eds.)
Corfu, Greece, 26–28 May 2011

THE EFFECT OF NON-SYNCHRONOUS SENSING IN WIRELESS SENSORS ON STRUCTURAL MODAL IDENTIFICATION

Zhouquan Feng[1], **Lambros S. Katafygiotis**[2]

[1] The Hong Kong University of Science and Technology
Clear Water Bay, Hong Kong, China
e-mail: simonce@ust.hk

[2] The Hong Kong University of Science and Technology
Clear Water Bay, Hong Kong, China
lambros@ust.hk

Keywords: non-synchronous sensing, wireless sensor network, modal identification.

Abstract. *Structural health monitoring (SHM) employing wireless sensor networks (WSN) is becoming increasingly popular in recent years. Accurate synchronized sensing amongst wireless sensors is a key issue enabling the implementation of such smart systems for SHM based on vibration measurements. However, perfect synchronized sensing is unachievable in WSN. The effect of non-synchronous sensing when using wireless sensors on structural modal identification is addressed and a methodology for correcting such errors is proposed herein. This paper first discusses the potential sources causing non-synchronous sensing and estimates their extents based on data samples collected from Imote2 sensors, and then investigates the impact of synchronization errors in the measured output response on modal identification using numerical simulations. The simulation results show that even small synchronization errors in the output response can distort the identified mode shapes. A new methodology is proposed herein for eliminating such errors. This methodology estimates the power spectral densities (PSDs) of output responses using non-synchronous samples directly based on a modified FFT. As long as the corrected PSDs are obtained, the correlation functions can also be easily obtained by IFFT. Then these corrected PSDs or correlation functions can be fed into various output-only modal identification algorithms. The proposed methodology is validated using numerical simulations. It is found that the simulation results closely match the identified parameters based on synchronous data.*

1 INTRODUCTION

In recent years, the emerging wireless sensor networks (WSN) for structural health monitoring (SHM) have attracted a lot of attention from both the academic and industrial communities [1].A wireless sensor network consists of a group of sensors using wireless links to perform distributed sensing and processing tasks. Compared with traditional wired sensor monitoring systems, there is no extensive wiring between sensors and data acquisition system involved, resulting in fast and flexible deployment, easier maintenance and cost reduction. In addition, wireless sensing technology allows sensor data to be processed locally at each sensor node, which can reduce the amount of data that needs to be transmitted and distribute the computing burden across the network. Inspired by these advantages, WSN are becoming even more popular in structural health monitoring applications.

Though WSN have the potential to improve SHM dramatically, a number of issues need to be addressed before wireless sensors can be utilized in SHM [2]. Time synchronization in WSN has been an important concern that has restricted the application of these networks since vibration-based SHM needs synchronous measured data. However, each wireless sensor in the network has its own intrinsic clock, and these clocks on the sensors have to be frequently synchronized with each other to maintain a consistent global time. For clock synchronization, several methods have been developed and tested [3]. The flooding time synchronization protocol (FTSP) [4] is adopted in our network, which is capable of clock synchronization with errors estimated to be about 10μs [5]. The clock synchronization is periodically performed to eliminate the clock offsets and skews. Thus, accurate clock synchronization among sensor nodes has been shown to be achievable.

However, even when the clocks on all sensor nodes are precisely synchronized, the measured signals may not be synchronized with each other due to the decentralized nature of WSN and resource limitations in each wireless sensor. In the following sections the potential sources causing non-synchronous sensing are first discussed and their extents are estimated using data collected from Imote2 sensors [6]. Then, the impact of non-synchronous sensing on modal identification is investigated by numerical simulations. A new methodology for eliminating such errors is proposed. Finally, the proposed methodology is validated by an illustrative example using simulated data.

2 SOURCES CAUSING NON-SYNCHRONOUS SENSING

Sensing on Imote2 sensors is performed in the following way. Prior to sensing, clock synchronization is conducted to convert the local clock times to global clock time using the estimated offsets and skews between local clocks and reference clock. Next the base station node sends sensing parameters such as sampling frequency and number of data points to remote nodes. When the prescribed start-sensing time arrives, sensing tasks are posted on the remote nodes. Once the sensing driver is ready, sensing starts. The sensing tasks continue running until the predetermined amount of data is acquired. During sensing, the acquired data points are first stored in a buffer. Every data point or every several data points can be marked with a local time stamp. When the buffer is filled, the data is passed to the sensing application for possible processing and/or transmission, and the emptied buffer becomes available for the next block of data. By examining the above sensing procedures, potential sources causing non-synchronous sensing are summarized below. A schematic diagram depicting these errors is shown in Figure 1.

(a). Clock synchronization error: for FTSP in Imote2 platform, this error is less than 10μs most of the time, with the maximum observed value being 80μs [5]. This error is comparatively small for SHM applications.

(b). Non-simultaneity in sensing start-up: starting sensing on all imote2 nodes simultaneously is challenging. Even if the time of start of sensing is set to be the same global time, the real execution time may have different delays in each node, and thus sensing may not start simultaneously.

(c). Differences in sampling frequency among sensor nodes: the actual sampling frequency may differ from the nominal value by at most 10 percent for the Imote2 Basic Sensor Board [7].

(d). Non-uniform sampling interval over time: a non-uniform sampling interval is observed in the Imote2 sensor boards. The coefficient of variation (COV) of the sampling interval is about 0.01~0.02%, which is relative small.

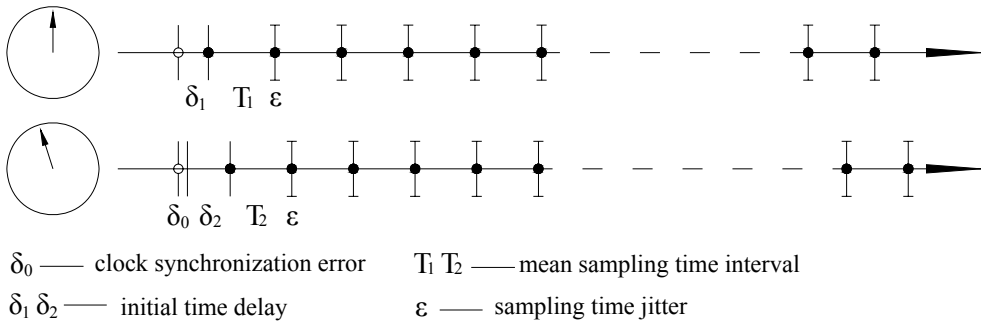

Figure 1: Illustration of non-synchronous sensing.

Ideally, the signal is sampled uniformly (with a constant sampling interval T_s) and synchronously (all the sensors start sensing at the same global time). The time at $(k+1)^{th}$ sampling instant is:

$$t_k = kT_s \tag{1}$$

Due to the reasons mentioned above, the $(k+1)^{th}$ data point is actually sampled at a different time instant:

$$t_k' = kT_s + \delta + ck + \varepsilon(k) \tag{2}$$

where, δ is a constant time shift, coming from sources (a) and (b); because the clock synchronization error is relatively small, only sensing start-up time delay is considered here; ck is a linear time shift, coming from source (c); the coefficient c is the difference between real sampling interval and nominal sampling interval; $\varepsilon(k)$ is a random time shift, coming from source (d), and these time jitters result in non-uniform sampling.

3 ERROR ESTIMATION

3.1 Test of non-synchronous sensing when using Imote2's

The extent of non-synchronous sensing when using Imote2's is evaluated using time stamps marked with data points when sampling. To evaluate these non-synchronous sensing errors, a group of ten Imote2 sensors were programmed with a sensing application. The sensing application was modified slightly from Illinois SHM Project (ISHMP) Services Toolsuite [8]. The sensor boards used are Imote2 basic sensor board ITS400B [6]. One sensor serves as base station node, the other nine sensors serve as remote nodes. After the base station node sends sensing parameters to these nine remote nodes, they start to sample at the same set time

and also record the time stamps of every data point. Processing these time stamps, we can estimate the non-synchronous sensing effect on Imote2 sensors. The statistical properties of the sampling times are listed in Table 1, and the differences of the start-sensing time among sensors are listed in Table 2.

node ID	mean sampling frequency (Hz)	mean sampling interval (μs)	% error $(\bar{\Delta t}_i - \Delta t_i)/\Delta t_i$	standard deviation of sampling interval	COV of sampling interval
3	38.64	25878	3.51%	3.0	0.01%
32	39.09	25584	2.33%	3.8	0.01%
98	38.20	26179	4.71%	3.7	0.01%
99	39.84	25099	0.40%	2.5	0.01%
101	40.50	24690	-1.24%	2.9	0.01%
102	40.47	24711	-1.16%	4.1	0.02%
104	39.22	25499	1.99%	4.6	0.02%
105	39.98	25011	0.04%	3.0	0.01%
113	38.77	25791	3.16%	5.2	0.02%

Notes: $\bar{\Delta t}_i, \Delta t_i$ are the actual mean sampling interval and the nominal sampling interval, respectively

Table 1: Statistics of sampling time (40Hz, 1000 points)

Node ID	3	32	98	99	101	102	104	105	113
relative time delay δ_i (μs)	14942	14160	16582	16582	8601	910	17908	10484	0
fractional time delay $\delta_i / \Delta t_i$	0.60	0.57	0.66	0.66	0.34	0.04	0.72	0.42	0

Table 2: Differences of the start-up time (Node 113 as reference)

From Table 1, we can see that the sampling frequencies of the accelerometers on the Imote2 sensor boards have various non-negligible deviations from the nominal value (40Hz), with a maximum of 4.71% error in Node #98. Differences in the sampling frequencies among the sensor nodes will result in inaccurate estimation of modal parameters unless appropriate post-processing is performed. From the last column in Table 1 we can see that the time intervals fluctuate about 0.01~0.02%, which is quite small, thus the non-uniform sampling effect (random shift term $\varepsilon(k)$) can be neglected. From Table 2 we can see that sensing start-up at all Imote2 sensor nodes is not simultaneous. Some of them start earlier and some later. Node #113 is the first one to start sensing, while Node #104 is the last one. Another observation is that these differences are all less than one sampling time interval. The maximum difference is 0.72 time step observed in Node #104. Although the commands to start sensing are set at exactly the same time, the execution times of the commands are different in different sensor nodes.

3.2 Effect of non-synchronous sensing on modal identification

The effect of time synchronization error on modal identification has been studied by Krishnamurthy et al. [12] and it was found that these errors affect the identified mode shape results. However, Krishnamurthy considered that these errors only come from clock synchronization errors and these errors have been overestimated. In reality, clock synchronization errors are comparatively small compared with other errors in Imote2 sensors.

To study the impact of synchronization errors on modal identification, we simulate a 2-DOF shear structural model subjected to white noise excitation. The 2-storey shear building model and the theoretical modal parameters (natural frequencies, modal shapes) are shown in Figure 2. In order to study the non-synchronous sensing effect, three cases of output response are considered: no time shift, constant time shift and linear time shift. According to the extent

of synchronization errors showed in section 3.1, the simulations of non-synchronous sensing are done using three scenarios: 1) Baseline (no time shift): both of the sampling frequencies are 40Hz; 2) Case1 (constant time shift): both of sampling frequencies are 40Hz, but channel #2 has 20000μs time delay; 3) Case2 (linear time shift): The sampling frequencies of channel #1 & #2 are 39.8406Hz & 40.4858Hz, respectively.

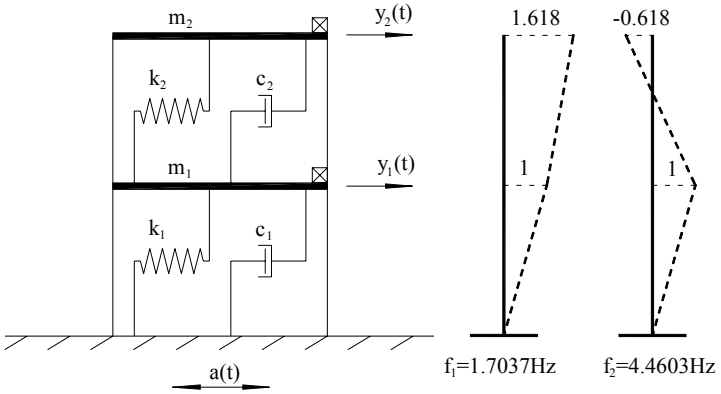

Figure 2: Two-storey shear structure

	Baseline: no shift		Case 1: constant shift		Case 2: linear shift	
	mode 1	mode 2	mode 1	mode 2	mode 1	mode 2
frequency (Hz)	1.7090	4.4824	1.7090	4.4824	1.7090	4.5020
%error	-	-	0.00%	0.00%	0.00%	0.44%
mode shape magnitude	1	1	1	1	1	1
	1.617	0.697	1.617	0.695	1.582	0.495
%error	-	-	0.00%	-0.29%	-2.16%	-28.98%
phase angle (°)	0	127	-12	94	-144	-105

Table 3: Comparison of identified modal parameters using PP method

	Baseline: no shift		Case 1: constant shift		Case 2: linear shift	
	mode 1	mode 2	mode 1	mode 2	mode 1	mode 2
frequency (Hz)	1.6992	4.4727	1.6992	4.4727	1.6797	4.5801
%error	-	-	0.00%	0.00%	-1.15%	2.40%
mode shape magnitude	1	1	1	1	1	1
	1.617	0.696	1.617	0.694	13.579	0.008
%error	-	-	0.00%	-0.29%	739.76%	-98.85%
phase angle (°)	0	127	-12	94	129	-115

Table 4: Comparison of identified modal parameters using FDD method

	Baseline: no shift		Case 1: constant shift		Case 2: linear shift	
	mode 1	mode 2	mode 1	mode 2	mode 1	mode 2
frequency (Hz)	1.7062	4.4593	1.7058	4.4832	1.7111	4.5032
%error	-	-	-0.02%	0.54%	0.29%	0.98%
mode shape magnitude	1	1	1	1	1	1
	1.615	0.526	1.600	0.589	0.257	0.006
%error	-	-	-0.93%	11.98%	-84.09%	-98.86%
phase angle (°)	0	-176	13	-155	108	53

Table 5: Comparison of identified modal parameters using NExT/ERA method

After obtaining the output response data of the structure, various modal identification algorithms can be applied to identify the modal parameters. In this study three popular output-only modal identification algorithms are utilized: Peak-Picking (PP) [9], Frequency Domain Decomposition (FDD) [10] and Natural Excitation Technique in conjunction with Eigensystem Realization Algorithm (NExT/ERA) [11]. The identified results are summarized and compared in Table 3, 4 & 5. It can be seen that all these three algorithms suffer from errors when using the non-synchronous samples directly. These errors affect only slightly the identified frequencies but affect the mode shapes considerably. The constant time shift error almost only affects the phase information of the mode shape. The linear time shift error has more influence on the modal parameters, especially the mode shapes, of which both the magnitude and phase suffer big errors. For these three output-only modal identification algorithms, FDD and NExT/ERA are more susceptible to synchronization errors, especially for linear time shift errors.

4 ERROR ELIMINATION

4.1 Proposed algorithm

In order to eliminate the synchronization errors, direct intuition suggests reconstructing the synchronous samples from measured non-synchronous ones. This is so called signal reconstruction, and some work has been done for this purpose such as interpolation based approach [13] and resampling based approach [5]. Nevertheless, such approaches can be computationally extensive. Rather than reconstructing the signal in the time domain, we develop a correction approach to recover the true spectral density using non-synchronous samples in the frequency domain. This approach is based on the spectral relationship of synchronous data and non-synchronous data. Because only spectral densities or correlation functions are needed for most of modal identification algorithms and raw synchronous time histories are not needed, reconstruction of the signal in the time domain is unnecessary. As long as we are able to obtain the corrected spectral densities, the correlation functions can also be easily obtained by IFFT.

4.1.1 Constant time shift

Consider two time histories $\{ x_\alpha(0), x_\alpha(\Delta t), \ldots x_\alpha((N\text{-}1)\Delta t)\}^T$ and $\{ x'_\beta(\delta), x'_\beta(\Delta t+\delta), \ldots x'_\beta((N\text{-}1)\Delta t+\delta)\}^T$, i.e., $\mathbf{x}'_\beta$ has a constant time shift δ. The discrete Fourier transform (DFT) for $\mathbf{x}_\alpha$ is given by

$$X_\alpha(\omega_k) = \sum_{n=0}^{n=N-1} x_\alpha(n\Delta t) e^{-j\omega_k n\Delta t} \tag{3}$$

where $\omega_k = k\Delta\omega$, $\Delta\omega = \dfrac{2\pi}{N\Delta t}$, $k = 0,1,...,\text{int}(N/2)$. The DFT for the shifted signal $\mathbf{x}'_\beta$ is given by

$$X'_\beta(\omega_k) = e^{j\omega_k\delta} \cdot X_\beta(\omega_k) \tag{4}$$

where $X_\beta(\omega_k)$ is the DFT of the original signal. Therefore,

$$X_\beta(\omega_k) = X'_\beta(\omega_k) \cdot e^{-j\omega_k\delta} = X'_\beta(\omega_k) \cdot \left(e^{-j\frac{2\pi}{N}\frac{\delta}{\Delta t}} \right)^k \tag{5}$$

Then, the true cross spectral density estimate can be obtained by

$$S_{x_\alpha x_\beta}(\omega_k) = \frac{\Delta t}{N} E[X_\alpha(\omega_k) X^*{}_\beta(\omega_k)] \tag{6}$$

where $(\cdot)^*$ denotes the complex conjugate operation.

4.1.2 Linear time shift

Consider two time histories $\{x_\alpha(0), x_\alpha(\Delta t_\alpha), \ldots x_\alpha((N_\alpha - 1)\Delta t_\alpha)\}^T$ and $\{x_\beta(0), x_\beta(\Delta t_\beta), \ldots x_\beta((N_\beta - 1)\Delta t_\beta)\}^T$, having different sampling frequencies, i.e. $\Delta t_\alpha \neq \Delta t_\beta$, with corresponding sampling time lengths $T_\alpha = N_\alpha \Delta t_\alpha$ and $T_\beta = N_\beta \Delta t_\beta$, respectively. In discrete Fourier transform, we know that $\omega_k = k\Delta\omega$ and $\Delta\omega = 2\pi / T = 2\pi / N\Delta t$. In order to ensure that $X_\alpha(\omega_k)$ and $X_\beta(\omega_k)$ correspond to the same discrete frequency when calculating the cross spectral density, their frequency resolutions should be identical, i.e., $\Delta\omega_\alpha \equiv \Delta\omega_\beta$, thus their duration time should be the same, i.e.,

$$N_\alpha \Delta t_\alpha = N_\beta \Delta t_\beta, \ \frac{N_\alpha}{N_\beta} = \frac{\Delta t_\beta}{\Delta t_\alpha} \tag{7}$$

Based on this relationship, the cross spectral density can be estimated by

$$S_{x_\alpha x_\beta}(\omega_k) = \frac{\Delta t_\beta}{N_\alpha} E[X_\alpha(\omega_k) X^*{}_\beta(\omega_k)] = \frac{\Delta t_\alpha}{N_\beta} E[X_\alpha(\omega_k) X^*{}_\beta(\omega_k)], \text{ when } N_\alpha, N_\beta \to \infty \tag{8}$$

where $\omega_k = k\Delta\omega$, $\Delta\omega = \dfrac{2\pi}{N_\alpha \Delta t_\alpha} = \dfrac{2\pi}{N_\beta \Delta t_\beta}$, $k = 0, 1, \ldots, \min\{\text{int}(N_\alpha / 2), \text{int}(N_\beta / 2)\}$.

4.1.3 Summary of proposed procedure

In reality, the time shifts of non-synchronous data are a combination of constant time shifts and linear time shifts. The most popular FFT-based method for power spectral density estimation is Welch's refined periodogram approach [14]. The procedures for computing the true power spectral density estimate from non-synchronous data in WSN are as follows:

(1) Calibrate the sampling frequencies of each sensor board before sensing experiment.

(2) Perform sensing experiment, and make sure the time stamps are also recorded when sampling.

(3) Set one sensor as reference and partition the data into several segments. Each segment has a length of N_r data points.

(4) Partition the data in other sensors into several segments as well. The first data point of each segment is chosen as close as possible to the first data point of the corresponding segment in the reference sensor data by comparing their time stamps. The length N_i of each segment is chosen such that the Eq. (7) holds approximately.

(5) Calculate the Fourier transform of each segment and correct it using Eq. (5).

(6) Calculate the cross spectral density using Eq. (8).

4.2 Numerical example

The structural system used is the same as before in section 3.2. The i^{th} sampling instant is chosen as follows: $t_1(i) = 0.0250 \times (i\text{-}1)$, $t_2(i) = 0.0247 \times (i\text{-}1) + 0.0200$, i.e. sensor #1 has a sam-

pling frequency 1/0.0250 (40) Hz, while sensor #2 has a slightly different sampling frequency 1/0.0247 (40.4858) Hz and a time delay 0.02 sec. The measurement noise for the response is taken to be 10 percent, i.e. the RMS of the measurement noise for a particular channel is equal to 10 percent of the RMS of the noise-free response at the corresponding channel.

The identified modal parameters using PP, FDD and NExT/ERA methods are summarized and compared in Table 6, 7 & 8. It can be seen that the modified methods using the proposed corrected spectral densities or correlation functions can achieve better accuracy than the original methods.

	Baseline (Synchronous Data)		Non-synchronous Data			
			Direct PP		Modified PP	
	mode 1	mode 2	mode 1	mode 2	mode 1	mode 2
frequency (Hz)	1.7090	4.4824	1.7090	4.4824	1.7090	4.4824
%error	-	-	0.00%	0.00%	0.00%	0.00%
mode shape magnitude	1	1	1	1	1	1
	1.617	0.703	1.498	0.553	1.625	0.684
%error	-	-	-7.36%	-21.34%	0.49%	-2.70%
phase angle (^{o})	0	131	174	-179	6	141

Table 6: Identified modal parameters (PP)

	Baseline (Synchronous Data)		Non-synchronous Data			
			Direct FDD		Modified FDD	
	mode 1	mode 2	mode 1	mode 2	mode 1	mode 2
frequency (Hz)	1.6992	4.4727	1.6797	4.5117	1.6992	4.4727
%error	-	-	-1.15%	0.87%	0.00%	0.00%
mode shape magnitude	1	1	1	1	1	1
	1.617	0.700	24.786	0.046	1.619	0.688
%error	-	-	1432.90%	-93.41%	0.14%	-1.79%
phase angle (^{o})	0	127	63	50	6	142

Table 7: Identified modal parameters (FDD)

	Baseline (Synchronous Data)		Non-synchronous Data			
			Direct NExT/ERA		Modified NExT/ERA	
	mode 1	mode 2	mode 1	mode 2	mode 1	mode 2
frequency (Hz)	1.7030	4.4660	1.7032	4.4770	1.7032	4.4509
%error	-	-	0.01%	0.25%	0.01%	-0.34%
mode shape magnitude	1	1	1	1	1	1
	1.614	0.545	0.062	0.007	1.629	0.451
%error	-	-	-96.14%	-98.80%	0.91%	-17.32%
phase angle (^{o})	0	-174	-78	-114	-6	-180

Table 8: Identified modal parameters (NExT/ERA)

5 CONCLUSIONS

The purpose of this paper is to address the problem of non-synchronous sensing on modal identification when using wireless sensor networks. The potential sources causing non-synchronous sensing are first discussed and their extents are estimated based on data collection from Imote2 sensors. Among these error sources the dominant ones are non-simultaneity in sensing start-up and differences in sampling frequency among sensor nodes. According to

numerical simulations, these errors can distort the identified results of the mode shapes. A new methodology is proposed for eliminating such errors. This methodology estimates the power spectral density (PSD) of output responses using non-synchronous samples based on a modified FFT. As long as we obtain the corrected spectral density, the correlation functions can also be easily obtained by IFFT. Then, these corrected PSDs or correlation functions can be fed into various output-only modal identification algorithms. Comparing with other existing methods of raw synchronous time history reconstruction, this methodology is simple and computationally efficient. The proposed methodology is validated using numerical simulations. The simulation results closely match the identified parameters based on synchronous data.

6 ACKNOWLEDGEMENTS

This research has been supported by the Hong Kong Research Grants Council under grant 614406. This support is gratefully acknowledged.

7 APPENDIX A – DERIVATION OF EQ(4)

The discrete Fourier transform for shifted $\mathbf{x}'_\beta$ is given by

$$\begin{aligned} X'_\beta(\omega_k) &= \sum_{n=0}^{n=N-1} x'_\beta(n\Delta t+\delta)e^{-j\omega_k n\Delta t} = \sum_{n=0}^{n=N-1} x'_\beta(n\Delta t+\delta)e^{-j\omega_k(n\Delta t+\delta)}\cdot e^{j\omega_k\delta} \\ &= e^{j\omega_k\delta}\cdot\sum_{n=0}^{n=N-1} x'_\beta(n\Delta t+\delta)e^{-j\omega_k(n\Delta t+\delta)} = e^{j\omega_k\delta}\cdot X_\beta(\omega_k) \end{aligned} \tag{9}$$

8 APPENDIX B – DERIVATION OF EQ(8)

The cross spectral density function between $\mathbf{x}_\alpha$ and $\mathbf{x}_\beta$ is defined by [15]

$$\begin{aligned} S_{x_\alpha x_\beta}(\omega_k) &= \lim_{T\to\infty}\frac{1}{T}E\left[X_\alpha(\omega_k,T)\cdot X^*{}_\beta(\omega_k,T)\right] \\ &= \lim_{T\to\infty}\frac{1}{T}E\left[\int_0^T x_\alpha(t)e^{-j\omega_k t}dt\cdot\left(\int_0^T x_\beta(t)e^{-j\omega_k t}dt\right)^*\right] \\ &= \lim_{T\to\infty}\frac{1}{T}E\left[\int_0^T x_\alpha(t)e^{-j\omega_k t}dt\cdot\int_0^T x_\beta(t)e^{j\omega_k t}dt\right] \\ &= \lim_{N_\alpha\to\infty}\frac{1}{N_\alpha\Delta t_\alpha}E\left[\Delta t_\alpha\sum_{n_1=0}^{N_\alpha-1}x_\alpha(n_1\Delta t_\alpha)e^{-j\omega_k n_1\Delta t_\alpha}\cdot\Delta t_\beta\sum_{n_2=0}^{N_\beta-1}x_\beta(n_2\Delta t_\beta)e^{j\omega_k n_2\Delta t_\beta}\right] \\ &= \lim_{N_\alpha\to\infty}\frac{\Delta t_\beta}{N_\alpha}E\left[\sum_{n_1=0}^{N_\alpha-1}x_\alpha(n_1\Delta t_\alpha)e^{-j\omega_k n_1\Delta t_\alpha}\cdot\sum_{n_2=0}^{N_\beta-1}x_\beta(n_2\Delta t_\beta)e^{j\omega_k n_2\Delta t_\beta}\right] \\ &= \lim_{N_\alpha\to\infty}\frac{\Delta t_\beta}{N_\alpha}E\left[X_\alpha(\omega_k)X^*_\beta(\omega_k)\right] \end{aligned} \tag{10}$$

REFERENCES

[1] J.P. Lynch, K.J. Loh, A Summary Review of Wireless Sensors and Sensor Networks for Structural Health Monitoring. *The Shock and Vibration Digest*, 38(2), 91-128, 2006.

[2] T. Nagayama, S.-H. Sim, Y. Miyamori, and B.F. Spencer Jr., Issues in Structural Health Monitoring Employing Smart Sensors. *Smart Structures and Systems*, 3(3), 299-320, 2007.

[3] B. Sundararaman, U. Buy, A.D. Kshemkalyani, Clock synchronization for wireless sensor networks: a survey. *Ad Hoc Networks*, 3(3), 281-323, 2005.

[4] M. Maróti, B. Kusy, G. Simon, Á. Lédeczi, The flooding time synchronization protocol. *Proceedings of the 2nd international conference on Embedded networked sensor systems*, Baltimore, MD, USA, November 3-5, 2004.

[5] T. Nagayama, B.F. Spencer Jr., *Structural Health Monitoring Using Smart Sensors*. Newmark Structural Engineering Laboratory Report Series 001, Available on: <https://www.ideals.illinois.edu/handle/2142/3521>, 2007.

[6] Crossbow Technology, Inc. Available on: < http://www.xbow.com/>.

[7] ST Microelectronics. Available on: < http://www.st.com/stonline/>.

[8] Illinois SHM Project (ISHMP) Services Toolsuite, Available on: < http://shm.cs.uiuc.edu/index.html>.

[9] A.J. Felber, *Development of a hybrid bridge evaluation system*. PhD Thesis, University of British Columbia (UBC), Vancouver, Canada, 1993.

[10] R. Brincker, L. Zhang, P. Andersen, Modal identification of output-only systems using frequency domain decomposition. *Smart Materials and Structures*, 10(3), 441-445, 2001.

[11] J.M. Caicedo, S.J. Dyke, E.A. Johnson, Natural Excitation Technique and Eigensystem Realization Algorithm for Phase I of the IASC-ASCE Benchmark Problem: Simulated Data. *Journal of Engineering Mechanics*, 130(1), 49-60, 2004.

[12] V. Krishnamurthy, K. Fowler and E. Sazonov, The effect of time synchronization of wireless sensors on the modal analysis of structures. *Smart Materials and Structures*, 17, 1-13, 2008.

[13] V. Divi, G. Wornell, Bandlimited signal reconstruction from noisy periodic nonuniform samples in time-interleaved ADCS. *Proceedings of IEEE International Conference on Acoustics, Speech and Signal Processing*, Las Vegas, NV, USA, March 30-April 4, 2008.

[14] P.D. Welch, The use of fast Fourier transform for the Estimation of Power Spectra: A Method Based on Time Aver- aging Over Short, Modified Periodograms. *IEEE Transactions on Audios and Electroacoustics*, AU-15, 70-76, 1967.

[15] J.S. Bendat, A.G. Piersol, *Engineering Applications of Correlation and Spectral Analysis*. John Wiley & Song, Inc. 1993.